Catalysts **2012**, *2*, 466-489; doi:10.3390/catal2040466

OPEN ACCESS

catalysts

ISSN 2073-4344

www.mdpi.com/journal/catalysts

Article

Tailoring Synthesis Conditions of Carbon Xerogels towards Their Utilization as Pt-Catalyst Supports for Oxygen Reduction Reaction (ORR)

Cinthia Alegre, David Sebastián, Estela Baquedano, María Elena Gálvez, Rafael Moliner and María Jesús Lázaro *

Institute of Carbochemistry, CSIC-Spanish National Research Council, C/. Miguel Luesma Castán, 4, 50018 Zaragoza, Spain; E-Mails: cinthia@icb.csic.es (C.A.); dsebastian@icb.csic.es (D.S.); estela.baquedano@gmail.com (E.B.); megalvez@icb.csic.es (M.E.G.); rmoliner@icb.csic.es (R.M.)

* Author to whom correspondence should be addressed; E-Mail: mlazaro@icb.csic.es; Tel.: +34-976-733-977; Fax: +34-976-733-318.

Received: 6 August 2012; in revised form: 24 September 2012 / Accepted: 9 October 2012 / Published: 17 October 2012

Abstract: Carbon xerogels characterized by different textural, structural and chemical properties were synthesized and used as supports for Pt catalysts for the application in polymer electrolyte fuel cells. Synthesis conditions were varied in order to synthesize carbon xerogels following the sol-gel method. These included the reactants ratio (precursor/formaldehyde), the catalyst concentration (precursor/catalyst ratio) and type (basic and acid), the precursor type (resorcinol and pyrogallol) and the solvent (aqueous or acetone based). Stoichiometric mixtures of resorcinol and formaldehyde yielded well polymerized gels and highly developed structures. Slow gelation, favored by the presence of acetone as solvent in the sol and low catalyst concentration, resulted in higher polymerization extent with a highly mesoporous or even macroporous texture and more ordered structure, as evidenced by XPS and Raman spectroscopy. Small Pt particles of *ca.* 3.5 nm were obtained by using carbon xerogels characterized by an ordered surface structure. The specific activity towards the oxygen reduction reaction, *i.e.*, the limiting catalytic process in low temperature fuel cells, is significantly favored by highly ordered carbon xerogels due to a metal-support enhanced interaction. Nevertheless, surface defects favor the distribution of the metallic particles on the surface of carbon, which in the end influences the effectiveness of the catalyst. Accelerated degradation tests were conducted to evaluate catalyst stability under potential cycling conditions. The observed decay of

performance was considerably lower for the catalysts based on ordered carbon xerogels stabilizing Pt particles in a higher extent than the other xerogels and the commercial carbon black support.

Keywords: carbon; xerogel; platinum; catalyst; oxygen; reduction; reaction

1. Introduction

Since their introduction by Pekala in 1989 [1], resorcinol–formaldehyde gels have been extensively studied. Numerous articles have appeared in recent literature describing the great variety of synthesis and processing conditions which lead to the production of organic and carbon gels such as aerogels, cryogels or xerogels—differing in the gel drying process: supercritically, freeze drying (maintain original gel porous structure) or subcritically—as well as how these conditions affect the final texture and structure of these materials [2]. It is generally observed that subcritical drying, *i.e.*, conventional drying, may result in a substantial collapse of the porous structure of the initial organic gel, however, if the synthesis conditions are appropriately chosen and the gel is mechanically strong enough to withstand capillary pressures, conventional drying can be carried out without involving major changes in the structure of the organic material [2]. Moreover, due to the possibility of fine-tuning their textural properties during the sol–gel process employed for their preparation, these materials have attracted enormous attention, given that one may change the ratio of micro-, meso- and macropores and, accordingly, their specific surface areas over a wide range, in order to tailor any particular application [3,4].

In particular, the uniqueness of the textural properties of these synthesis-tailored carbon materials include high porosity (>80%), high surface area (400–1200 m^2 g^{-1}) and controlled pore size distributions (1 to 50 nm). These properties are fundamental requires in the application of carbon materials as supports in the preparation of catalytic systems, especially within the field of fuel cell technologies [5,6]. In fact, depending on the application, pore size distribution can play a definitive role in catalytic activity and stability. The presence of micropores has been reported to be efficient in hosting the active sites, *i.e.* in the preparation of iron based catalysts [7,8]. Moreover, pore structure in fuel cell electrodes affects mass transportation of fuel and exhausts, highly affecting the fuel cell performance [9]. Several studies point out the key importance of a macro- mesopore enriched porous structure in carbon materials for fuel cells mass transportation processes [9–11]. This fact stands out as a unique advantage of using carbon gels as electrocatalyst supports, moreover in comparison to the mostly microporous carbon blacks normally used in the preparation of the commercially available catalytic systems. For instance, Arbizzani *et al.* [12] developed PtRu catalysts, prepared by both chemical and electrochemical routes, on mesoporous cryo- and xerogel carbons. The specific catalytic activity of these catalysts was found to significantly increase; almost doubling the one measured using Vulcan carbon black instead, even in passive DMFC configuration. Job *et al*. [13] synthesized several platinum catalysts supported on different carbon xerogels and tested their activity in the oxygen reduction reaction (ORR), comparing their performance with that of analogous carbon aerogels' supported catalysts. They determined that some carbon xerogels supported catalysts presented comparable activities to carbon aerogels, and that the metal surface available for the oxygen reduction

reaction and the voltage losses due to diffusion phenomena strongly depend on the carbon pore texture. The same research group [14] further improved the catalysts synthesis method by using a strong electrostatic adsorption method and tested the catalysts as cathodes in PEM fuel cells. The cathode activity, expressed as a function of the mass of Pt involved, was found to double the one measured for the previously presented catalysts, prepared by impregnation with H_2PtCl_6 and reduction in aqueous phase by $NaBH_4$. Guilminot *et al.* [15] developed new nanostructured carbons through pyrolysis of organic aerogels, based on supercritical drying of cellulose acetate gels. These cellulose acetate-based carbon aerogels were activated by CO_2 at 800 °C, subsequently impregnated with $[PtCl_6]^{2-}$, and submitted to either chemical or electrochemical reduction. The oxygen reduction reaction kinetic parameters of the carbon aerogel supported Pt, determined from quasi-steady-state voltammetry, were comparable with those of Pt/Vulcan XC-72R. Liu and Creager [16] prepared Pt catalysts supported on carbon xerogels as electrodes for PEM fuel cells, determining that Pt/CX possessed slightly higher intrinsic catalyst activity at low current density (0.9 V cell voltage) given its slightly higher Pt particle size when compared to Pt/Vulcan-XC-72R. Cell performance (after normalization for Pt loading) at higher current densities was slightly higher for Pt/CX, what may reflect a possible lower mass transfer resistance in the case of using carbon xerogels as catalysts supports.

In the present work, different carbon xerogels (CXs) were prepared varying the synthesis conditions (reactant molar ratio, solvent, catalyst amount/type and precursor) in order to determine the particular role of the different textural, structural and chemical properties of the carbon xerogels. The activity towards the oxygen reduction reaction (ORR), occurring in the cathode compartment of polymer electrolyte fuel cells, as well as the resistance to potential cycling degradation was evaluated for the carbon xerogel-supported Pt electrocatalysts.

2. Results and Discussion

2.1. Influence of Synthesis Conditions in the Textural Properties of Carbon Xerogels

Though it will be further on described in detail within the experimental section, note that the synthesized carbon xerogels were labelled as follows: CX stands for carbon xerogel, followed by an identifying number and the main variable changed in its synthesis. For instance: CX-1-RF-25, stands for a carbon xerogel prepared under a resorcinol/formaldehyde molar ratio = 0.25. Carbon xerogels named as CX-4-RC-50-Ac. or CX-5-H_2SO_4, were synthesized under resorcinol/catalyst molar ratio = 50, using acetone as solvent and sulphuric acid as catalyst, respectively. Carbon xerogels followed by RC-800-W or RC-1500-W represent carbon materials synthesized with a resorcinol/catalyst molar ratio = 800 or 1500, and water (W) as solvent. Vulcan XC-72C carbon black, denoted C-Vulcan, was also used in the preparation of analogous catalytic systems.

Table 1 shows the values of BET surface area (S_{BET}), micropore volume (V_{micro}), mesopore volume ($V_{meso\ BJH}$), total pore volume ($V_{pore\ p/p_0 \approx 1}$), as well as mean pore diameter, derived from the N_2 adsorption isotherms acquired for the carbon xerogels prepared under different synthesis conditions. The results obtained in this textural characterization confirm that carbon materials of diverse porous structures can be obtained by modifying parameters such as the precursor to formaldehyde molar ratio (P/F), the amount and type of catalyst and solvent employed. The assorted values of surface area

obtained, ranging from 176 to 554 m^2 g^{-1}, clearly indicate that carbon xerogels possess different degrees of porous structure development, resulting in materials with very different pore size distribution.

Table 1. Surface area and pore volumes obtained from N_2 adsorption isotherms for the carbon xerogels prepared.

Carbon xerogel	S_{BET} (m^2 g^{-1})	V_{micro} (cm^3 g^{-1})	$V_{meso\ BJH}$ (cm^3 g^{-1})	$V_{pore\ p/p_0 \approx 1}$ (cm^3 g^{-1})	Mean pore size (nm)
CX-1-RF-25	554	0.09	0.82	0.93	8.9
CX-2-RF-50	534	0.12	0.95	1.07	11.7
CX-3-RF-100	176	0.10	0.00	0.10	3.4
CX-4-RC-50-Ac	425	0.19	0.16	0.39	10.9
CX-5-H_2SO_4	390	0.21	0.01	0.23	2.6
CX-6-RC-800-W	528	0.14	1.66	1.79	23.1
CX-7-RC-1500-W	405	0.22	0.04	0.27	11.6
CX-8-Pyrogallol	234	0.12	0.01	0.14	24.0
C-Vulcan	224	0.04	0.46	0.47	11.0

Carbon xerogels CX-1-RF-25, CX-2-RF-50 and CX-3-RF-100 were prepared using different resorcinol to formaldehyde molar ratios. Moving to R/F (resorcinol/formaldehyde) molar ratios lower than the stoichiometric value of 0.5, results in excess formaldehyde and, thus, increased reactant dilution, which yields higher polymeric particle sizes near the gelation limit [2]. Thus, upon drying, the gel structure partially collapses, resulting in a material, CX-1-RF-25, possessing lower mean pore size and lower mesopore, V_{BJH}, pore volume, in comparison to CX-2-RF-50, carbon xerogel synthesized using the stoichiometric molar ratio. Tamon and co-workers previously reported similar collapse of the mesopore structure, due to the presence of remaining formaldehyde after sol-gel polycondensation [17]. Further increasing *R*/*F* molar ratio up to a value of 1, *i.e.*, excess resorcinol, results in a carbon material, CX-3-RF-100, which is predominantly microporous. Tamon *et al.* described as well difficulties in drying the gel prepared using *R*/*F* = 1, due to incomplete gelation of the sol. Maldonado-Hódar *et al.* [18] reported lower surface areas and pore volume corresponding to pore diameter higher than 50 nm, for carbon aerogels synthesized using increasing R/F molar ratios. Final textural properties of the carbon xerogels are as well determined by the relative amount of catalyst in the sol. Catalysts act in fact as a buffer regulating the sol pH. In the case of using an alkaline catalyst, *i.e.*, Na_2CO_3, it is generally considered that low P/C (precursor/catalyst) molar ratios result in small polymer particles (about 3–5 nm size) which are highly interconnected by large necks giving the gel a fibrous appearance. In contrast, high P/C molar ratios result in large polymer particles (16–200 nm diameter), yielding a carbon material of notably increased mesopore volume [2]. A low amount of catalyst, *i.e.*, high P/C ratios, means fewer nucleation sites in the sol for the growth of clusters, which thus form a less branched network and will persist longer in the nucleation regime, leading to less compact gels [19,20]. In this sense, CX-6-RC-800-W, synthesized using P/C = 800, possesses higher mesoporous volume and shows increased mean pore size in comparison to CX-2-RF-50, prepared at P/C = 50. However, further increase of P/C molar ratio from 800 to 1500 leads to a carbon xerogel, CX-7-RC-1500-W, of increased micropore volume, with almost no contribution of mesopores, in comparison to the materials synthesized at P/C values of 50 and 800, most probably due to the presence of wide pores (>300 nm),

or macropore-enriched structure. On the other hand, employing an acid catalyst—H_2SO_4—in the synthesis of these materials, see CX-5-H_2SO_4, results in faster gelation [2], leading to a highly cross-linked and thus more dense structure which yields a completely microporous carbon material. Solvent type, *i.e.*, using acetone instead of water: compare CX-4-RC-50-Ac to CX-2-RF-50 , the latter synthesized using P/C = 50 and water as solvent, results in a more controlled evaporation due to lower surface tension of acetone in comparison to water. Moreover, most probably the presence of acetone in the media slows down the gelation rate yielding higher primary particle size less compact gel, to a much lesser extent, but having a similar effect than the increase in P/C ratio. The carbon xerogel synthesized using pyrogallol as precursor, instead of resorcinol, CX-8-Pyrogallol, possesses a poorly developed porous structure, as previously reported by El Mir *et al*. [21].

2.2. Influence of Synthesis Conditions in the Structural Properties of Carbon Xerogels

Figure 1 shows the C 1s band in the XPS spectra acquired for the different carbon xerogels prepared. These C 1s bands were deconvoluted into five components [22]. The contribution at 284.5-284.6 eV can be ascribed to the presence of C-C bonds in graphitic carbon. A peak at *ca.* 284.9-285.3 eV is related to the presence of defects in the graphitic structure of the carbon material. Whereas, peaks at *ca.* 286.7 eV and 287.8 eV account for the presence of oxidized carbon, in the form of C-O and C=O species, respectively. Finally, a low intensity and broad band at *ca.* 290 eV is traditionally attributed to π-π^* transition characteristic of pure graphitic samples, sometimes considered as an indirect measure of the graphitic character of carbon blacks. Many differences can be observed at the sight of the C 1s bands shown in Figure 1, which point to important dissimilarities among the prepared carbon materials, as a function of their particular synthesis conditions. In most cases, C-C peak at 284.5-284.6 eV is accompanied by a significant contribution corresponding to functionalized C; C-O and C=O peaks, in fact, generate a band which even appears as a separated peak, and not as a shoulder contribution to C-C signal, contrary to what could be expected in a relatively ordered carbon material, see for example Figure 1 h, C 1s band for Vulcan carbon black. These contributions corresponding to functionalized C can be due to incomplete or too fast and random gelation of the organic gel mixture, due either to reactant excess, to excess catalysts or to the use of acidic catalysts, leading to the presence of an important fraction of non-polymerized material which upon pyrolysis is transformed into amorphous/disordered/defected carbon. In this sense, the amount of catalyst employed within the synthesis seems crucial. CX-6-RC-800-W and CX-7-RC-1500-W present C 1s bands with a marked C-C contribution, in comparison to CX-2-RF-50, moreover compared to CX-1-RF-25, CX-3-RF-100 or CX-5-H_2SO_4.

Raman spectra, shown in Figure 2, confirm the results obtained in the deconvolution of XPS C 1s signal of the synthesized carbon materials. Raman spectroscopy is a well-known technique revealing short-range structural order changes in carbon materials. A Raman spectrum of perfect graphite shows a single narrow first order peak at 1580 cm^{-1} known as G band, ascribed to the stretching of C–C bonds in the hexagonal rings [23,24]. However, in imperfect graphite, G band is usually accompanied by another band at about 1360 cm^{-1} known as D band that has been normally associated to the presence of defects in the graphite structure, and thus known as “defect band”. The variation in the position, width and relative intensities of D and G bands in Raman spectra are therefore characteristic

of structural differences in carbon materials. In this sense, it is well-known that the position of G band is shifted to higher frequencies, the width of D band increases and the intensity ratio I_D/I_G raises as the short-range structural order in graphite decreases. Spectra obtained for the various carbon xerogels considered in this work are presented in Figure 2. All the carbon materials show a wide D band, whose intensity is relatively similar to that of G band, shifted in all cases to higher frequencies around 1585–1595 cm^{-1}. Relative intensity of these bands, I_D/I_G, is however lower for CX-4-RC-50-Ac and, more evidently, in the case of CX-6-RC-800-W and CX-7-RC-1500-W. The low amount of catalyst used in the synthesis of this two carbon materials resulted, as explained before, in slower gelation, less dense and lower cross-linked but highly polymerized organic gel, which upon pyrolysis yields a slightly more organized carbon material presenting a lower number of structural defects.

Figure 1. XPS C 1s band and deconvolution for the different carbon xerogels prepared (**a**–**h**), and Vulcan carbon black (**h**).

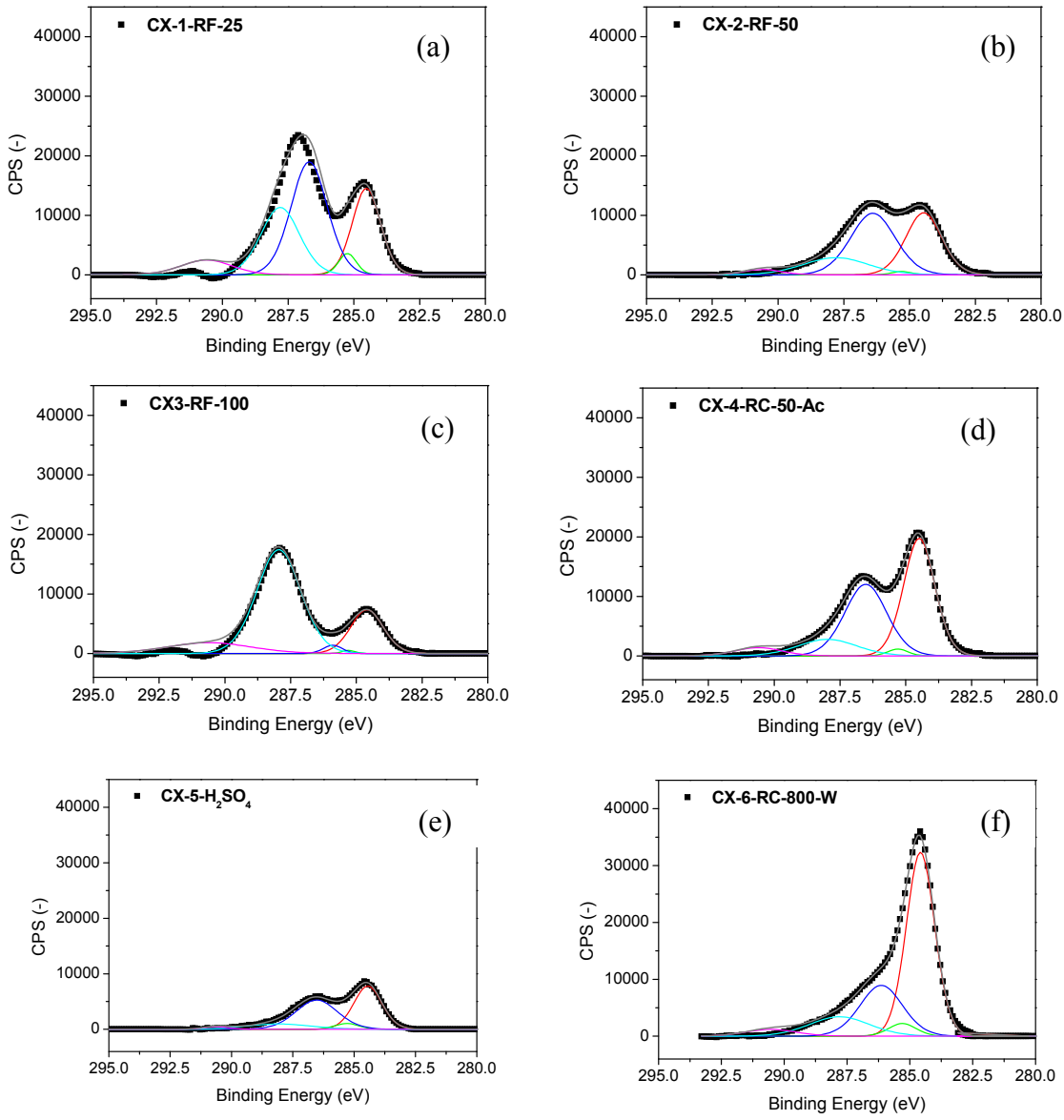

Figure 1. *Cont.*

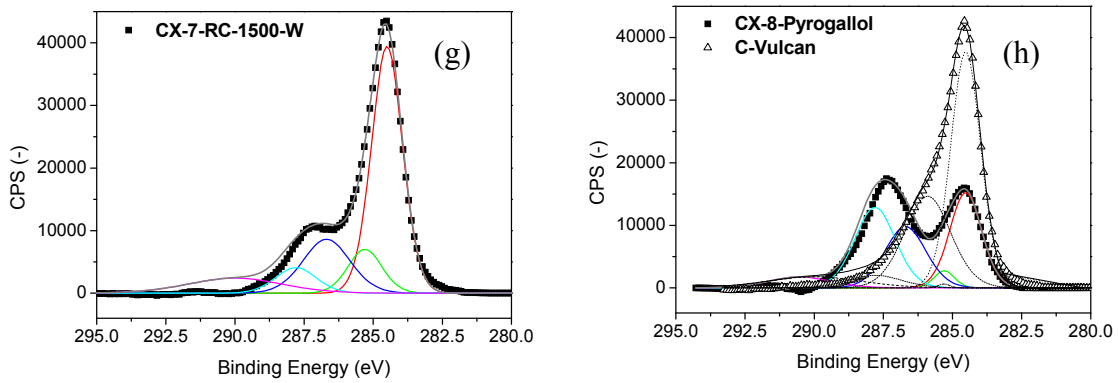

Figure 2. Raman spectra acquired for the synthetized carbon xerogels and Vulcan carbon black.

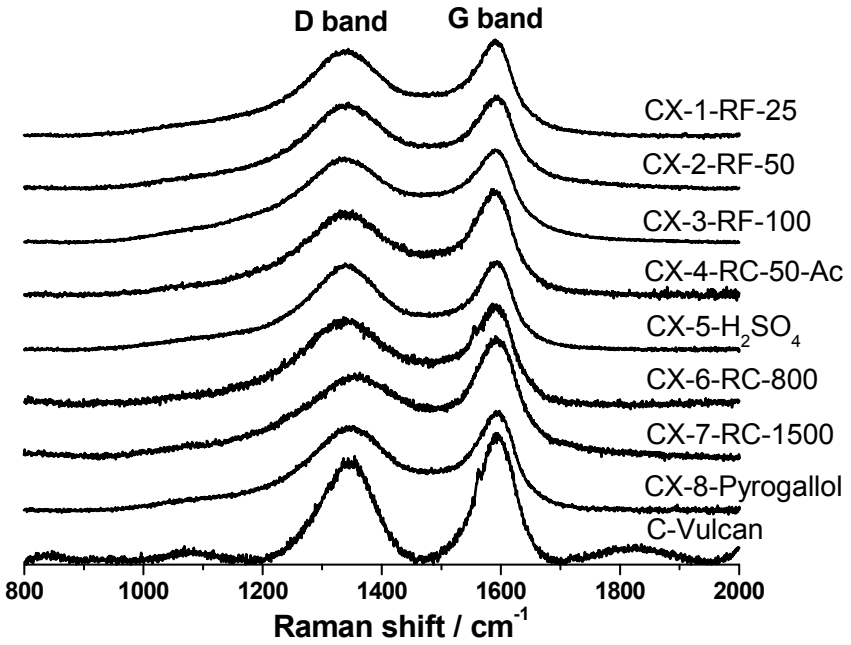

Further evidence on the higher degree of ordering in some of the synthesized materials can be gained through the measurement of their electrical conductivity. Figure 3 presents the conductivity measured, as a function of the applied pressure, for several carbon xerogels synthesized under different conditions. In agreement with the results obtained in the characterization of these materials by means of XPS and Raman spectroscopy, carbons CX-6-RC-800-W and CX-7-RC-1500-W show higher conductivity within the pressure interval, pointing to a less defected structure. The inset in Figure 3 plots the conductivity measured for Vulcan carbon black, compared to the synthetic carbon materials, evidencing much higher conductivity for this carbon black than for any of the synthesized carbon xerogels, due to its well-known highly ordered structure, both in terms of short and long range order.

Figure 3. Electric conductivity *vs*. pressure for some of the prepared carbon xerogels; insert presents the conductivity of Vulcan carbon black as a function of the pressure, in comparison to the same series of carbon materials.

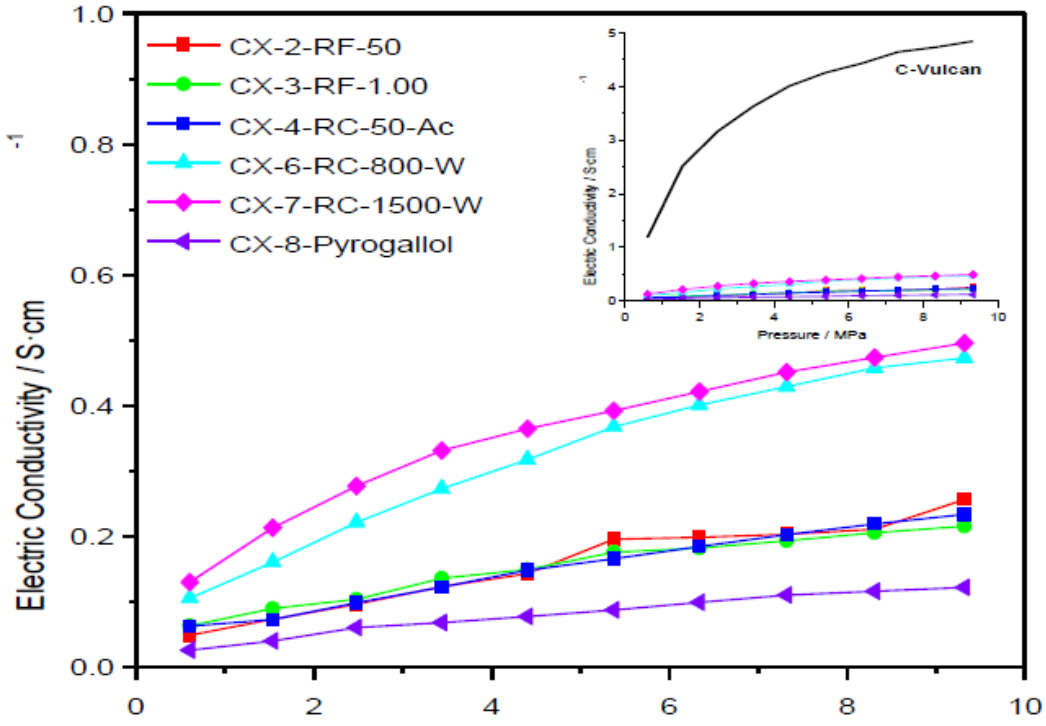

2.3. Surface Chemistry of the Carbon Materials

Table 2 shows the results of the deconvolution of the TPD profiles, as well as the oxygen content calculated both from TPD experiments and from the integration of XPS O 1s signal of the different carbon materials studied. The series of synthesized carbon xerogels slightly differ in their oxygen content, which is higher when calculated by means of XPS than out of TPD experiments, *i.e.*, TPD predicts O contents from 1.1 to 4.0% wt. whereas XPS allowed the calculation of O contents between 9.5 and 14.3% wt, as expected (XPS only accounts for the surface whereas TPD is a bulk technique), but following the same trend. It is worth noting that higher oxygen content was determined for the carbon xerogels synthesized using pyrogallol as precursor, CX-8-Pyrogallol, and those prepared using P/C ratio of 50. Increasing P/C to 800 and 1500, see CX-6-RC-800-W and CX-7-RC-1500-W, results in somehow lower oxygen contents, in agreement as well with lower contribution of functionalized C in C 1s XPS signals determined for these materials. In comparison to the synthetic carbon xerogels, Vulcan carbon black possesses significantly lower oxygen content, 0.6% wt. according to TPD and 6.4% wt. according to XPS. With respect to the deconvolution of TPD profiles, no clear influence can be observed regarding the variation of the different synthesis parameters on the particular presence of oxygen surface groups of a certain type. Most of the carbon materials possess a surface enriched in thermally more stable carbonyl/quinone-type and phenolic groups, though in some cases the amount of strongly acidic carboxylic functionalities results remarkable, such as in the case of CX-2-RF-50, CX-8-Pyrogallol or CX-3-RF-100.

Table 2. Oxygen content from XPS and TPD, as well as surface oxygen groups composition obtained from the deconvolution of the CO and CO_2 TPD profiles for the carbon supports.

Carbon material	Oxygen content (% wt.)		Cbx *	Anh *	Lac *	Ph *	Cbn/Qn *
	XPS	TPD					
CX-1-RF-25	12.8	2.2	0.12	0.06	0.11	0.17	0.57
CX-2-RF-50	12.1	1.9	0.33	0.01	0.08	0.10	0.23
CX-3-RF-100	14.3	4.0	0.49	0.09	0.22	0.52	0.27
CX-4-RC-50-Ac	10.5	2.7	0.10	0.14	0.10	0.34	0.57
CX-5-H_2SO_4	11.4	1.7	0.06	0.06	0.04	0.23	0.46
CX-6-RC-800-W	9.5	1.7	0.16	0.02	0.06	0.31	0.26
CX-7-RC-1500-W	9.7	2.4	0.08	0.09	0.05	0.25	0.75
CX-8-Pyrogallol	14.2	1.1	0.14	0.01	0.13	0.05	0.07
C-Vulcan	6.4	0.6	0.00	0.00	0.18	0.00	0.00

* **Cbx**: Carboxylic, **Anh**: Anhydride, **Lac**: Lactone, **Ph**: Phenolic, **Cbn/Qn**: Carbonyl/Quinone surface groups, in mmol/g.

2.4. Solid-State Characterization of Pt-Catalysts

The different carbon xerogels synthesized were used as Pt-catalysts supports, in order to evaluate the influence of the carbon material textural and structural properties in the electrochemical performance of these catalysts in the electrochemical oxygen reduction reaction (ORR).

Table 3 shows the results obtained in the textural characterization of the carbon xerogel and Vulcan carbon black supported Pt-catalysts. As previously described elsewhere [25], Pt is deposited mostly on the mesoporous structure of the carbon materials. Therefore, an important decrease of mesopore volume can be observed in most cases, amounting to almost 45% loss of mesopore volume, $V_{\text{meso BJH}}$, in the case of CX-6-RC-800-W. It is worth noting that in the case of Pt/CX-7-RC-1500-W and contrary to what could be expected, mesopore volume increases from 0.04 to 0.21 $cm^3\ g^{-1}$ upon Pt loading. This increase is due to partial blockage of wide mesopores or macropores reaching a size lower than 300 nm. To a lower extent, this can be as well observed for CX-4-RC-50-Ac and CX-8-Pyrogallol. Still, generally, most of the catalysts maintain an adequately developed porous structure after the deposition of the active phase, moreover in comparison with the analogous catalyst prepared using Vulcan carbon black as support.

XPS was used to identify the oxidation state of Pt on the surface of the different catalysts prepared. Pt 4f core level region was curve fitted to three sets of spin-orbital doublets, namely accounting for $4f_{7/2}$ and $4f_{5/2}$ peaks. Contributions at 71.4, 72.7 and 75.1 eV, and 74.8, 76.1 and 78.4 eV, were assigned to Pt^0, Pt^{2+} (PtO) and Pt^{4+} (PtO_2) oxidation states, respectively, based on the existing literature on XPS studies of carbon-based Pt and PtRu catalysts [26–28]. Full-width at the half-maximum, FWHM, and relative intensities of such species are presented in Table 4. For most catalysts, Pt^0 was found to be the predominant species on their surface. There is, however, an important contribution of oxidized Pt^{2+}, as well as of Pt^{4+}. Lower amount of Pt^0 can be found, according to XPS, in the catalysts prepared using the supports CX-1-RF-25, CX-2-RF-50 and CX-3-RF-100. The more difficult and less

effective Pt deposition in such cases can be ascribed to the poorly developed and defect-full structure of these series of carbon materials, as well as to the increased presence of carboxylic groups on their surface. Surface chemistry must in fact play a decisive role during the impregnation process. Indeed, the catalyst prepared using the carbon xerogel CX-5-H_2SO_4, possessing the lower amount of carboxylic functionalities on its surface, see TPD deconvolution in Table 2, presents an increased presence of reduced Pt, the highest of this series, 73.6%, in comparison to 43.5% determined for Pt/CX-3-RF-100.

Table 3. BET surface area and pore volumes obtained from N_2 adsorption isotherms for the Pt-catalysts prepared.

Carbon xerogel	S_{BET} (m^2 g^{-1})	V_{micro} (cm^3 g^{-1})	$V_{meso\ BJH}$ (cm^3 g^{-1})	$V_{pore\ p/p_0 \approx 1}$ (cm^3 g^{-1})	Mean pore size (nm)
Pt/CX-1-RF-25	476	0.08	0.76	0.84	10.9
Pt/CX-2-RF-50	472	0.13	0.71	0.84	10.0
Pt/CX-3-RF-100	-	-	-	-	-
Pt/CX-4-RC-50-Ac	306	0.14	0.18	0.33	11.6
Pt/CX-5-H_2SO_4	-	-	-	-	-
Pt/CX-6-RC-800-W	380	0.14	0.94	1.08	23.5
Pt/CX-7-RC-1500-W	314	0.14	0.21	0.38	11.6
Pt/CX-8-Pyrogallol	116	0.06	0.03	0.10	23.2
Pt/C-Vulcan	173	0.03	0.35	0.38	11.9

- Not available.

Table 4. Deconvolution of XPS Pt $4f_{7/2}$ signal for the different catalysts prepared.

Catalyst	Pt $4f_{7/2}$			
	Species	B.E. (eV)	FWHM (eV)	Intensity (%)
Pt/CX-1-RF-25	Pt	71.4	1.5	48.0
	PtO	72.8	2.4	41.2
	PtO_2	75.1	3.2	10.8
Pt/CX-2-RF-50	Pt	71.3	1.5	40.1
	PtO	72.9	2.4	45.3
	PtO_2	75.0	3.2	14.6
Pt/CX-3-RF-100	Pt	71.3	1.5	43.5
	PtO	72.9	2.4	33.2
	PtO_2	75.0	3.2	23.3
Pt/CX-4-RC-50-Ac	Pt	71.4	1.5	57.8
	PtO	72.7	2.4	37.6
	PtO_2	75.1	3.2	4.6
Pt/CX-5-H_2SO_4	Pt	71.4	1.5	73.6
	PtO	72.7	2.5	22.8
	PtO_2	75.0	3.2	3.6

Table 4. *Cont.*

Catalyst	Pt $4f_{7/2}$			
	Species	B.E. (eV)	FWHM (eV)	Intensity (%)
Pt/CX-6-RC-800-W	Pt	71.5	1.5	65.6
	PtO	72.7	2.4	26.8
	PtO_2	75.1	3.1	7.6
Pt/CX-7-RC-1500-W	Pt	71.5	1.5	66.8
	PtO	72.7	2.4	16.3
	PtO_2	75.1	3.1	16.9
Pt/CX-8-Pyrogallol	Pt	71.5	1.5	66.6
	PtO	72.7	2.4	30.2
	PtO_2	75.1	3.1	3.2
Pt/C-Vulcan	Pt	71.5	1.5	59.2
	PtO	72.7	2.4	27.9
	PtO_2	75.1	3.1	12.9

X-ray diffraction patterns of the various catalysts are shown in Figure 4. Platinum showed face centered cubic structure. Pt crystal sizes were calculated from the Pt (220) peak broadening and applying the Scherrer's equation, and the values are reported in Table 5. Small Pt particles of about 3.5 nm were obtained for the catalysts based on CX-4-RC-50-Ac, CX-6-RC-800-W and CX-7-RC-1500-W, this is, the carbon xerogels characterized by stoichiometric resorcinol/formaldehyde ratio. The rest of supports gave place to higher Pt crystal sizes of *ca.* 5 nm, and even higher in the case of the carbon xerogel based on pyrogallol as precursor (8.4 nm). It must be pointed out here that the platinum concentration was the same for all these catalysts, as determined by ICP-AES, evidencing that the differences encountered in crystal size may not be ascribed to different platinum loadings. Moreover, neither the BET surface area of the support nor the surface oxygen content explains this trend of Pt particle size. It must then be interpreted in terms of surface morphology and defects. It is well known that platinum nucleation and growth takes place preferentially at defect carbon sites [29]. Pt crystals became bigger in the case of carbon xerogel supports based on a higher density of defects, as evidenced by weaker C-C signal in C 1s XPS band and higher values of I_D/I_G determined by Raman spectroscopy, pointing to lower extent of polymerization resulting in a less ordered gel structure. The Pt crystal size for Vulcan carbon-black supported catalysts is also small and accordingly similar to those carbon xerogels with a low density of defects, *i.e.*, CX-4-RC-50-Ac, CX-6-RC-800-W and CX-7-RC-1500-W.

According to the Pt crystal size of these catalysts, a selection was considered to investigate the electrochemical activity towards the oxygen reduction reaction (ORR). This reaction is governed by the Pt crystal size, showing a volcano-shaped curved with a maximum at approximately 3 nm, as demonstrated by Kinoshita [30]. For this reason, the catalysts showing a Pt crystal size close to 3.5 nm were chosen, this is, those based on CX-4-RC-50-Ac, CX-6-RC-800-W and CX-7-RC-1500-W supports as well as Vulcan carbon black-based catalyst.

Figure 4. Diffractograms obtained by XRD for the synthesized Pt catalysts.

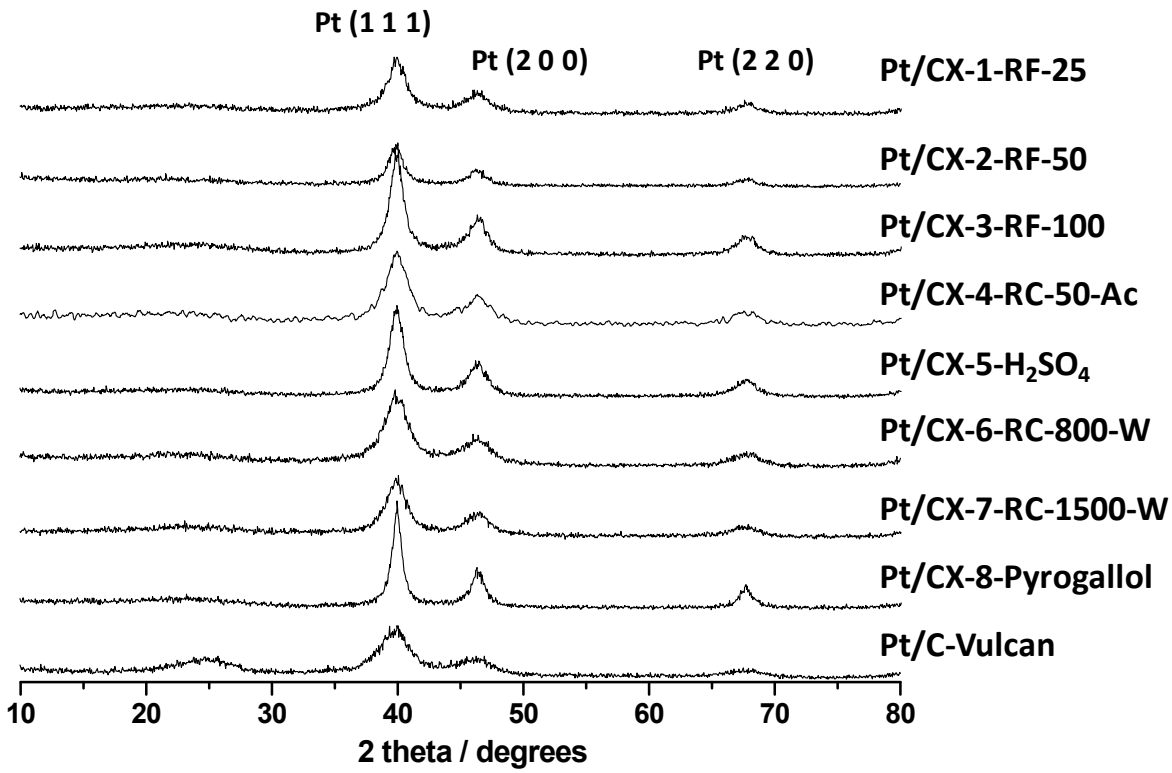

Table 5. Pt crystal size obtained by XRD and Pt concentration in the synthesized catalysts.

Catalyst	Crystal size (nm)	% wt. metal concentration
Pt/CX-1-RF-25	5.1	19.9
Pt/CX-2-RF-50	5.3	16.9
Pt/CX-3-RF-100	5.2	15.8
Pt/CX-4-RC-50-Ac	3.6	20.5
Pt/CX-5-H_2SO_4	5.2	23.5
Pt/CX-6-RC-800-W	3.6	17.9
Pt/CX-7-RC-1500-W	3.7	18.6
Pt/CX-8-Pyrogallol	8.4	21.7
Pt/C-Vulcan	3.4	16.7

2.5. Catalytic Activity towards ORR and Durability Tests

The catalytic activity towards the oxygen reduction reaction (ORR) was determined by polarization curves for the selected catalysts in a half-cell system under a continuous flow of pure oxygen, using 0.5 M sulfuric acid as electrolyte and at 25 °C. Figure 5 shows the polarization curves obtained for the three selected carbon xerogel based catalysts. It is worth to mention that the three of them present a very similar slope in the low current density region, this is, the activation controlled part of the polarization curve, although the catalytic activity at a determined potential value is maximized for the catalyst based on CX-6-RC-800-W. Similar slopes indicate that the oxygen adsorption mechanism is

essentially the same, corresponding to a Temkin type adsorption process, according to the values calculated from Tafel plots (approx. 70–80 mV dec^{-1}), removing the contribution of ohmic drop. This electrokinetic parameter evidences the similar Pt particle size of approx. 3.6 nm and appropriate nanoparticles dispersion. Slight differences encountered at low current density are more evident at high current density (higher overpotential). The catalyst with the highest mass activity (A g^{-1}_{Pt}) is the one based on CX-6-RC-800W, this is, the one based on xerogels with a high porosity development (Table 3). This support is characterized by a wide pore size (23.5 nm) in comparison with the other xerogels (11.6 nm) and the commercial support (11.9 nm) and also a high mesopore volume (0.94 cm^3 g^{-1}). These results highlight the importance of support morphology and porosity on the electrochemical activity, which may result a key parameter for the operation in a fuel cell cathode [5,6].

Figure 5. Polarization curves obtained in gas diffusion electrode, 0.5 M H_2SO_4 electrolyte, feeding pure oxygen to the backing layer and at 25 °C.

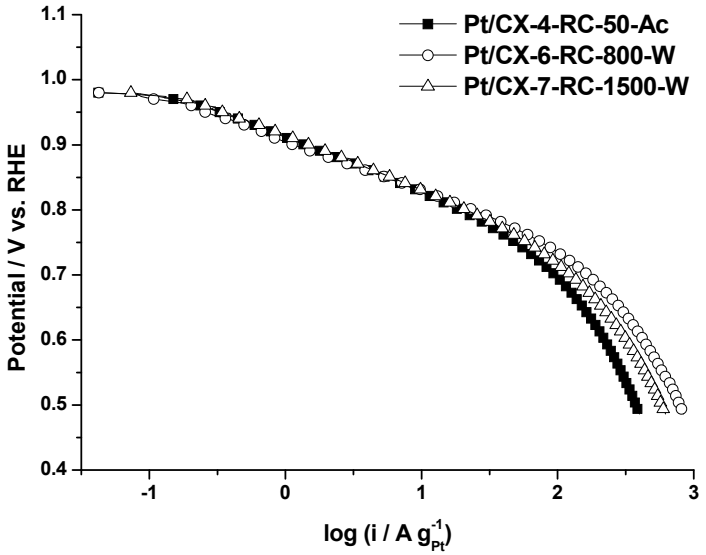

The selected Pt-catalysts were subjected to an accelerated test procedure to evaluate catalyst stability under potential cycling conditions. Figure 6 shows an example of accelerated degradation test (ADT) for the catalyst Pt/CX-4-RC-50-Ac. All the electrodes followed the same trend and are not included for simplicity. It can be clearly observed how the oxygen reduction peak (negative current peak at around 0.07 V *vs.* MSE) shifts to higher potentials and decreases in intensity during the cycling process (from the first cycle to the 1000th cycle as indicated by the arrows). This can be attributed to an increase of particle size with the consequent reduction of the electrochemically active surface area (ECSA), and an increase of the specific (or intrinsic) activity for oxygen reduction, as observed by Aricò and co-workers [31]. The decrease of the electrochemically active surface area is also evidenced in the cyclic voltammograms recorded at room temperature in 0.5 M H_2SO_4, represented in Figure 7. The hydrogen adsorption-desorption region, this is, the response at potentials between −0.60 and −0.40 V *vs.* MSE, clearly shows the change in the ECSA after the accelerated degradation test. It must be noted that as carbon xerogels present a relatively high BET surface area, the contribution of the double layer

capacitance to current values is significantly higher than that commonly obtained for carbon blacks with an approximately two-fold lower BET surface area. The appearance of a small oxidation-reduction response (−0.30 to +0.05 V *vs.* MSE) suggests the formation of oxygen groups on the surface of carbon support, which also indicates that the catalyst stability may be influenced not only by the Pt particle growth (presumably due to Ostwald ripening mechanism) but also by the corrosion of carbon support, which may lead to Pt particles instability. To individuate the contribution of both main degradation phenomena (Pt growth and carbon corrosion), XRD analysis may indicate the Pt crystal size growth, but the total amount of Pt in the corroded area of the electrodes is not high enough (less than 20 µg) to obtain reliable results. Future works with larger electrode areas will be performed to identify the degradation mechanisms.

Figure 6. Accelerated Pt degradation test by potential cycling for Pt/CX-4-RC-50-Ac, 1000 cycles in 0.5 M H_2SO_4 at room temperature.

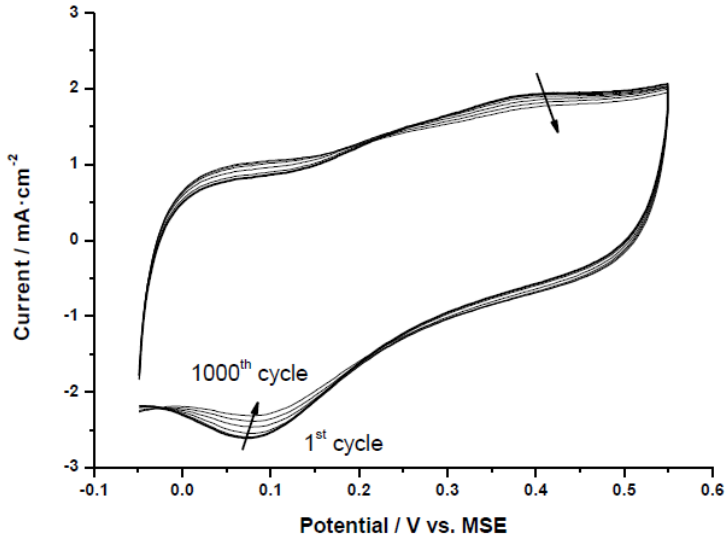

Figure 7. Cyclic voltammetry (half-cell, nitrogen fed, 0.5 M H_2SO_4, 25 °C) before and after accelerated degradation tests (ADT) for the catalyst Pt/CX-4-RC-50-Ac.

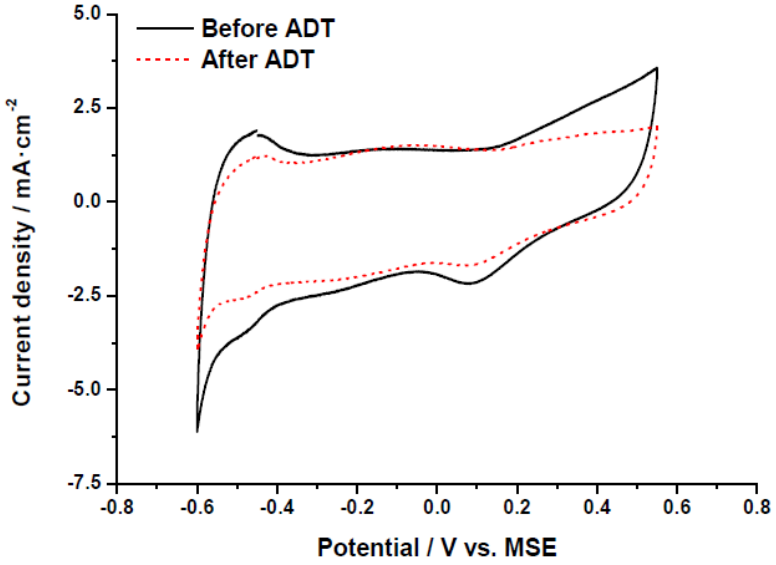

The electrochemical activity towards the ORR was evaluated by polarization curves in half-cell, as further described in the experimental section. Figure 8 shows the polarization curves for the catalyst Pt/CX-4-RC-50-Ac before and after the ADT, as an example. The same behavior was obtained for all the catalysts, indicating that, after the degradation, the catalytic activity decreases as a result of several phenomena (Pt particle growth, Pt loss, support corrosion, *etc.*). It must be pointed out that the values of mass activity have been obtained under flooded conditions, at room temperature and sulfuric acid, so these performances cannot be directly comparable to those obtained in polymer electrolyte fuel cells. To individuate the causes of this activity loss as well as to evaluate the catalytic activity as a function of the carbon xerogel properties, cyclic voltammetry and polarization curves were analyzed before and after the ADT.

Figure 8. Polarization curves (half-cell, oxygen fed, 0.5 M H_2SO_4, 25 °C) before and after accelerated degradation tests (ADT) for the catalyst Pt/CX-4-RC-50-Ac.

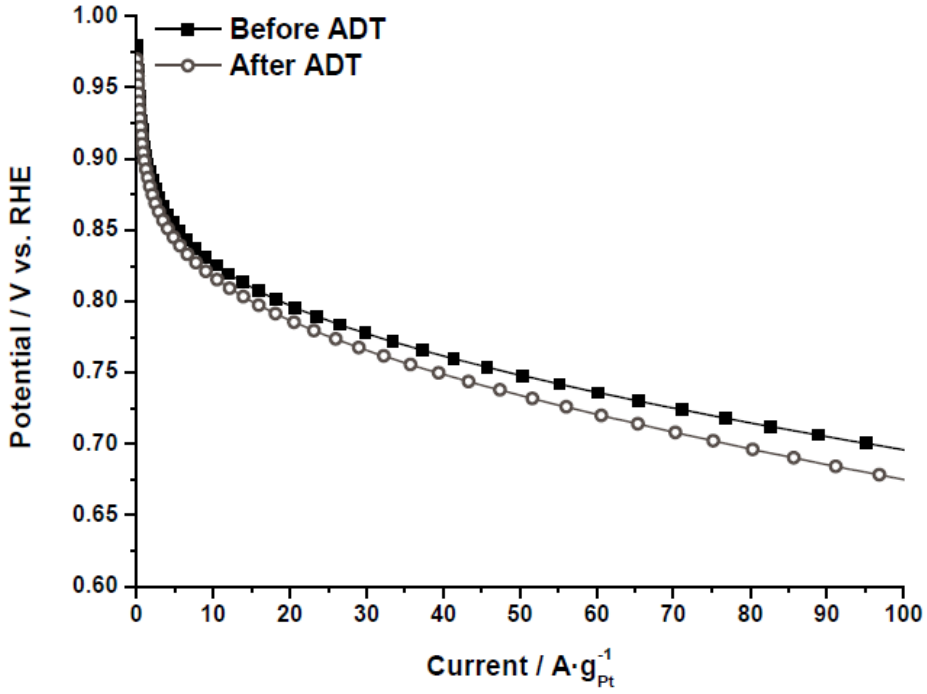

Figure 9 shows the values of ECSA before and after the degradation procedures. The highest ECSA was found for Vulcan as support and a clear tendency for the decrease of surface area from CX-4-RC-50-Ac to CX-7-RC-1500-W was observed. These results are interpreted in terms of the distribution of Pt particles on the support, as all of them present very similar Pt particle size as evidenced from XRD (Table 5) of about 3.5 nm, and similar metal concentration. Comparing carbon black and carbon xerogels, platinum dispersion is not favored by the BET surface area of the support but by the presence of a moderate concentration of surface functional groups that act as particle agglomeration centers rather than properly dispersing the metal particles [32]. However, the presence of surface defects on carbon xerogels seems to better distribute Pt particles on the surface. This is also evidenced in TEM observations. Representative TEM captions can be observed in Figure 10. The catalysts presented a unimodal Pt particle size distribution very close to that determined by XRD, but significant differences were encountered among them with respect to the distribution of particles. Whereas the catalyst based

on the less structured support, this is CX-4-RC-50-Ac presents a rather homogeneous distribution of particles, some agglomerates were formed, also evidenced by carbon surface not covered by Pt, with the increase of carbon ordering, in good agreement to the variation previously discussed of ECSA values.

After the degradation tests, the relative decrease of ECSA is the lowest for the sample based on the carbon xerogel with the highest ordering degree, this is, CX-7-RC1500-W where the ECSA not only does not decrease but it is slightly higher after the ADT. The ripening effect, this is, the dissolution and reprecipitation of Pt particles may cause an increase of metal available Pt atoms in surface which is in practice translated into the improvement of ECSA for this particular sample. Catalysts based on less ordered carbon xerogel supports experience a notably decrease of ECSA. This evidences the need of using ordering support surface to maximize Pt stability under severe cyclic potential corrosion.

Figure 9. Electrochemically active surface area (ECSA) before and after accelerated degradation tests (ADT).

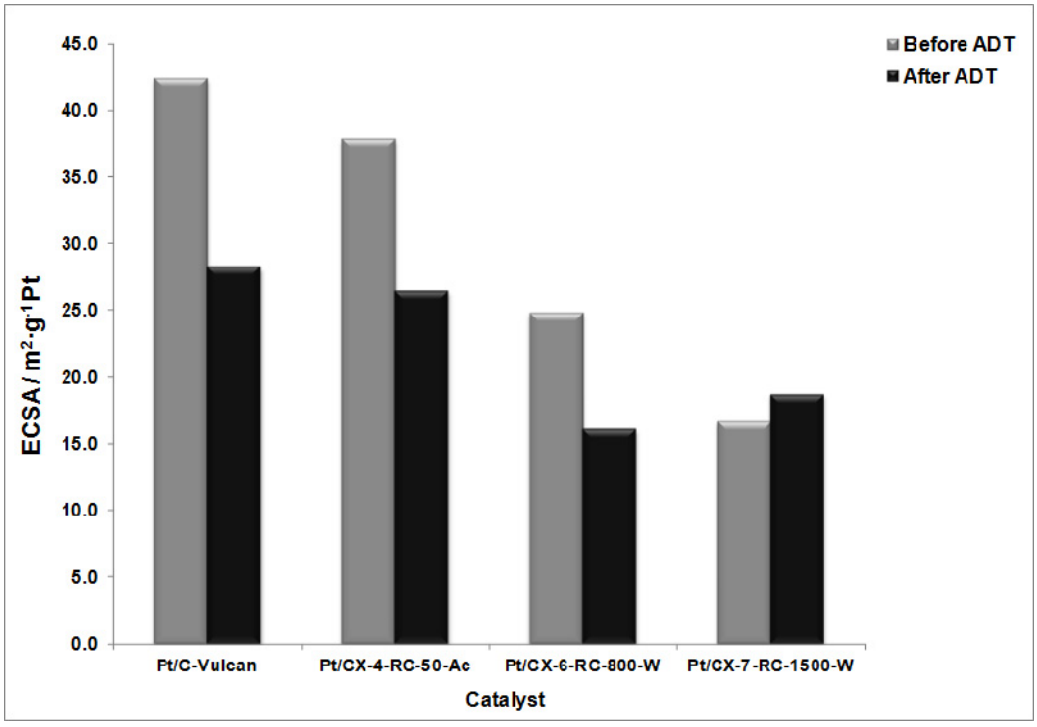

Figure 11 shows the specific or intrinsic activity for all the catalysts in the activation controlled region of the polarization curves, this is, at low current densities and/or high potential (0.80 V *vs.* RHE). The current values were normalized with respect to the Pt electrochemically active surface area obtained from the hydrogen desorption region in the cyclic voltammograms. According to the Kinoshita theory, the specific activity increases as the relative number of faceted (111) Pt atoms increases, which is directly related to the particle size. The higher the Pt particle size, the higher the specific activity. Nevertheless, the catalysts studied present very similar Pt particle size (*ca.* 3.5 nm), being slightly shifted in the right branch of the Kinoshita's volcano-shaped curve [30]. This suggests that the encountered differences in specific activity must be attributed to different metal-support interaction when varying the support features. Indeed, the specific activity progressively increases with the surface ordering of carbon xerogels, being maximized for the catalyst based on CX-7-RC-1500-W, characterized by a less defected structure, evidenced by means of XPS C 1s signal and Raman

spectroscopy. Moreover, the specific activity is almost two-fold higher for the catalyst based on CX-7-RC-1500-W compared to the catalyst based on the conventional carbon black (Vulcan). Pt oxidation state, see deconvolution of XPS Pt $4f_{7/2}$ signal presented in Table 4, might be also playing a certain role, *i.e.*, Pt^0 content in these catalysts follows the same trend than their specific activity: 59.2% for Pt/C-Vulcan, 57.8% for Pt/CX-4-RC-50-Ac, 65.6% for Pt/CX-6-RC-800-W and 66.8% for Pt/CX-7-RC-1500.

Figure 10. Representative TEM micrographs of the various electrocatalysts (**a**) Pt/CX-4-RC-50-Ac (**b**) Pt/CX-6-RC-800-W and (**c**) Pt/CX-7-RC-1500-W.

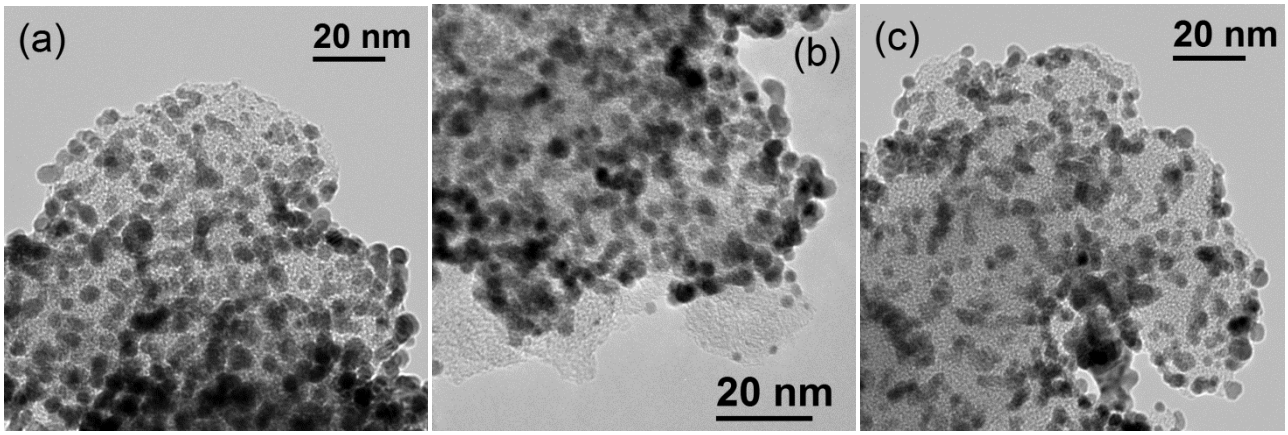

Figure 11. Specific activity at 0.80 V *vs*. RHE (half-cell, oxygen fed, 0.5 M H_2SO_4, 25 °C) before and after accelerated degradation tests (ADT).

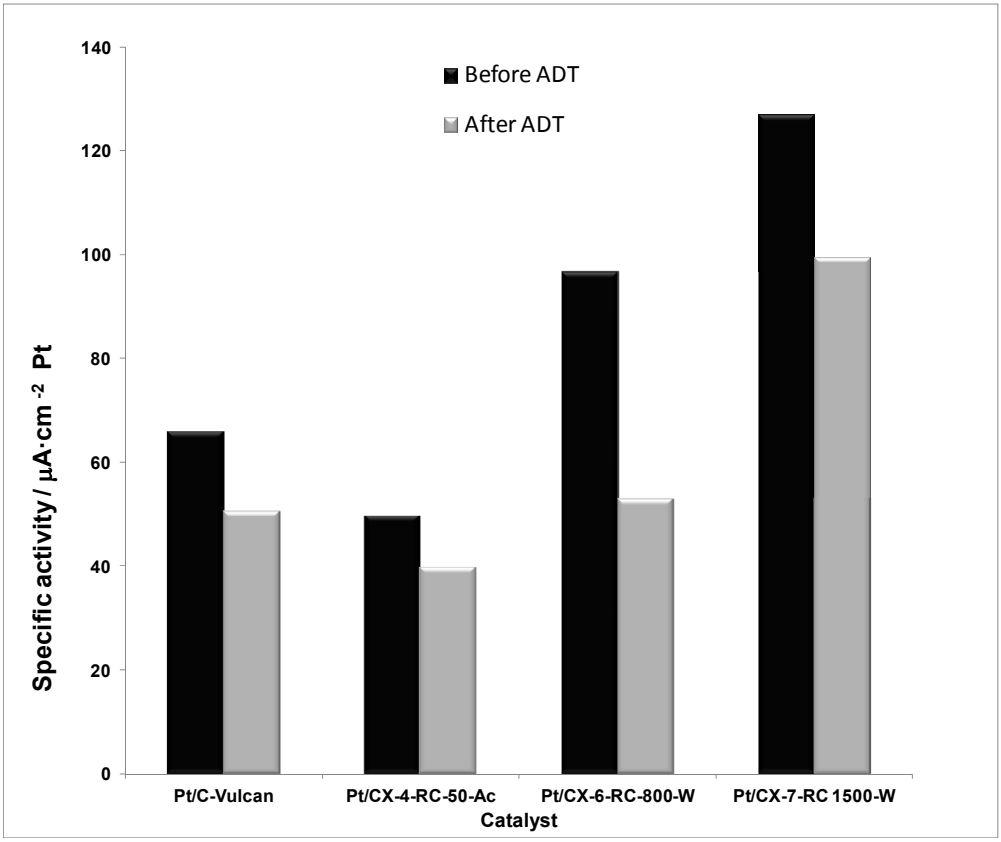

The mass activities, this is, the current values normalized by the Pt mass content, are reported in Figure 12. As a result of combining the effect of ECSA and specific activity, the mass activity is maximized when using a carbon xerogel with intermediate properties. This is the case of CX-6-RC-800-W. On one hand, the electrochemical surface area is favored by using carbon xerogels characterized by a higher density of surface defects, which may presumably favor the average number of Pt active sites for the electroreduction of oxygen. On the other hand, the low electrochemical surface area is in part compensated by a high specific activity. The ordering degree of carbon favors the metal-support interaction, as evidenced by XPS results, considerably increasing the intrinsic activity. As a result, carbon xerogels with intermediate properties result of high interest for both distribution of particles and activity reasons.

Figure 12. Mass activity at 0.80 V *vs*. RHE (half-cell, oxygen fed, 0.5 M H_2SO_4, 25 °C) before and after accelerated degradation tests (ADT).

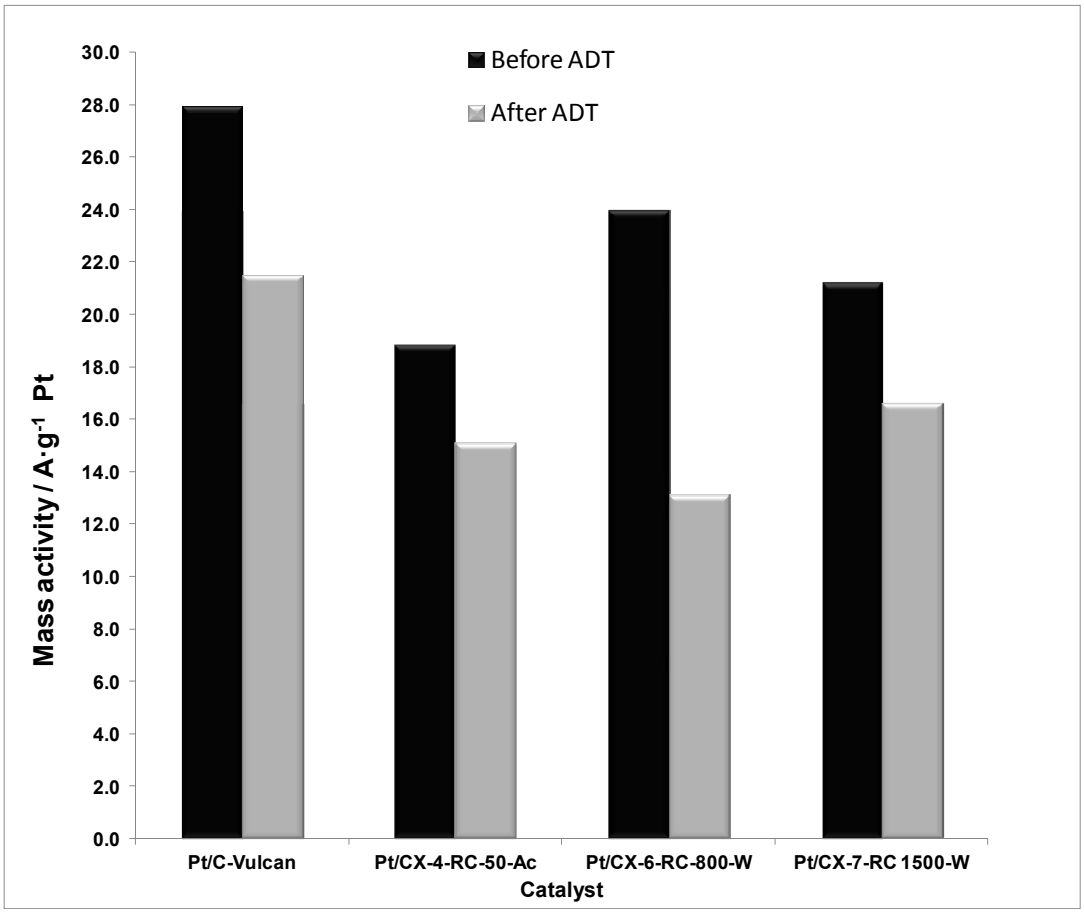

When considering the relative activity loss after ADT procedures, the catalyst based on the carbon xerogel with high ordering degree presented the lowest loss of activity, attributed both to the slight increase of electrochemical surface area and the stabilization of Pt particles as evidenced from the lower relative loss of specific activity. Consequently, the appropriate carbon support must not be selected only in terms of its initial activity, but considering also the expected life-time of the fuel cell.

3. Experimental Section

3.1. Carbon Xerogel Synthesis

Resorcinol (1,3-dihydroxybenzoic acid)-formaldehyde organic gels were synthesized following the sol-gel method originally proposed by Pekala *et al*. [1]. Two different precursors, resorcinol and pyrogallol, and two different catalysts, Na_2CO_3 and H_2SO_4, were used. The molar ratio precursor (P)/formaldehyde (F) was modified in the synthesis of the different xerogels, as well as the molar ratio precursor (P)/catalysts (C). Either deionized water or acetone, were used as solvents. Table 6 shows the different synthesis parameters used for each of the carbon xerogels prepared. Briefly, reactants were mixed in the corresponding amounts and, after 30 min stirring, were poured in closed vials, and kept for 24 h at room temperature. The vials were then placed in a muffle at 50 °C for the next 24 h. Finally, temperature was increased up to 85 °C and maintained during 120 h curing time. Hydrogels were subcritically dried in an oven for 5 h at 65 °C and 5h at 110 °C. Pyrolysis of the xerogels thus obtained was carried out in a tubular furnace at a temperature of 800 °C for 3 h under a N_2 flow of 100 mL/min.

Table 6. Carbon xerogel synthesis parameters.

Sample name	Precursor	P/C[(1)]	P/F[(2)]	Catalyst	Solvent
CX-1-RF-25	Resorcinol	50	0.25	Na_2CO_3	Water
CX-2-RF-50	Resorcinol	50	0.50	Na_2CO_3	Water
CX-3-RF-100	Resorcinol	50	1.00	Na_2CO_3	Water
CX-4-RC-50-Ac	Resorcinol	50	0.50	Na_2CO_3	Acetone
CX-5-H_2SO_4	Resorcinol	50	0.50	H_2SO_4	Water
CX-6- RC-800-W	Resorcinol	800	0.50	Na_2CO_3	Water
CX-7- RC-1500-W	Resorcinol	1500	0.50	Na_2CO_3	Water
CX-8- Pyrogallol	Pyrogallol	0.33	0.33	H_2SO_4	Water

(1) Precursor (P)/Catalyst (C) molar ratio;(2) Precursor (P)/Formaldehyde (F) molar ratio.

3.2. Catalysts Preparation

Pt was deposited on the synthesized carbon xerogels and on Vulcan XC-72R carbon black (for comparison purposes) by means of impregnation and reduction with formic acid. The amount of metallic precursor (H_2PtCl_6) was calculated to obtain a metal loading of 20% *w*/*w*. Each carbon material was first dispersed in a 2 M HCOOH solution at 80 °C. Subsequently an aqueous solution of H_2PtCl_6 (Sigma-Aldrich) was added dropwise. Finally catalysts were filtered, thoroughly washed with ultrapure water, and dried overnight at 60 °C.

3.3. Physico-Chemical Characterization

The textural and morphological features of the different carbon supports and catalysts prepared were determined by means of nitrogen physisorption at −196 °C (Micromeritics ASAP 2020), scanning electron microscopy (SEM, Hitachi S-3400 N) and transmission electron microscopy (JEOL JEM-2000 FX II). Textural properties such as specific surface area, pore volume and pore size

distribution were calculated from each corresponding nitrogen adsorption-desorption isotherms applying the Brunauer-Emmet-Teller (BET) equation, Barrett-Joyner-Halenda (BJH) and t-plot methods. Raman spectra of carbon xerogels were obtained with a Horiba Jobin Yvon HR800 UV, using the green line of an argon laser (λ = 514.53 nm) as excitation source. The carbon ordering degree was evaluated by means of the relative intensities of D (*ca.* 1350 cm^{-1}) and G (*ca.* 1590 cm^{-1}) peaks. Electrical conductivity measurements were performed pressing the carbonaceous powder at 10 MPa as described elsewhere [32]. The electrical resistance was measured applying electrical currents up to 0.02 A. Surface chemistry of carbon supports was studied by temperature-programmed desorption. Such experiments were performed in a Micromeritics Pulse Chemisorb 2700 equipment, under a flow of argon with a heating rate of 10 °C min^{-1} from 150 °C up to 1050 °C. The amounts of CO and CO_2 desorbed from the samples were analyzed by gas chromatography in a HP 5890 chromatograph with a thermal conductivity detector, packed columns Porapak N 10 ft and molecular sieve. These experiments give information about the surface oxygen groups created during the oxidation treatments. Acidic groups (carboxylic groups, lactones and anhydrides) are decomposed into CO_2 at low temperatures and basic and neutral groups (anhydrides, phenols and quinones) are decomposed into CO at high temperatures [33]. Gaussian function was used to fit each functional group contribution and the corresponding addition of Gaussian curves was fitted minimizing the square of the deviations by a numerical routine as described elsewhere [34]. Inductively coupled plasma atomic emission spectroscopy (ICP-AES) was used to determine the amount of metal deposited. Catalysts were as well characterized by X-Ray Diffraction (XRD), using a Bruker AXS D8 Advance diffractometer, with a θ-θ configuration and using Cu-Kα radiation. Crystallite sizes were calculated from the Scherrer's equation on the (2 2 0) peak for platinum. X-ray photoelectron spectrometry (XPS) analysis were performed using a ESCAPlus Omicron spectrometer equipped with a Mg (1253.6 eV) anode, 150 W (15 mA, 10 kV) power, over an area of sample of 1.75 × 2.75 mm. C 1s (280–295 eV), O 1s (526–540 eV) and Pt 4f (65–84 eV) signals were obtained at 0.1 eV step, 0.5 s dwell and 20 eV pass energy. Spectra were deconvoluted using CasaXPS software.

3.4. Electrochemical Experiments

Gas diffusion electrodes were prepared according to a procedure described elsewhere [35], consisting of carbon cloth backing, gas diffusion layer and the catalytic layer under study. To reduce the flooding effects in the sulfuric acid half-cell, a hydrophobic backing layer was used (LT 1200W ELAT, E-TEK). The catalytic layer was composed of 33 wt.% Nafion® ionomer and 67 wt.% catalyst, with a Pt loading of *ca.* 0.10 mg cm^{-2} (±0.02 mg cm^{-2}).

Half-cell tests were carried out in a conventional thermostated three-electrode cell consisting on the gas diffusion electrode to be tested (working electrode), a mercury-mercurous sulfate reference electrode (Hg/Hg_2SO_4, sat.) and a high surface coiled platinum wire as counter electrode. The electrode geometric area was 0.2 cm^2, and a 0.5 M H_2SO_4 aqueous solution was employed as electrolyte. Gas (nitrogen or oxygen) was fed to the electrode backing layer during the tests. A μAutolab Metrohm potentionstat/galvanostat was used to perform the measurements. Among the various methods reported in literature [36], an accelerated stress test has been selected for the evaluation of the catalysts resistance to degradation. It consists on a continuous potential cycling

between 0.6 and 1.2 V *vs*. RHE up to a total of 1000 cycles, feeding nitrogen to the electrode. The evaluation of the decay process was carried out by in situ electrochemical tests: cyclic voltamperometry (from 0.02 to 1.2 V *vs*. RHE) in nitrogen and polarization curves in pure oxygen.

4. Conclusions

Carbon xerogels were synthesized varying several parameters within their preparation procedure, such as precursor to formaldehyde ratio, solvent, catalyst amount and type, as well as substituting resorcinol by pyrogallol as precursor. The carbon materials synthesized possess very different textural, structural and chemical features, which ultimately determined the characteristics and electrochemical behavior of the Pt catalysts prepared using them as supports. Synthesis conditions of the gels strongly influence the textural properties of the final carbon material. Non-stoichiometric mixtures of resorcinol and formaldehyde yielded partially polymerized gels of weak and poorly developed structure. Faster gelation in the presence of an acidic catalyst resulted in a too compact gel, with a low extent of development of its porous structure. Pyrogallol also resulted in a very dense and almost non-porous material. On the other hand, an increase in resorcinol/catalyst molar ratio resulted in slower gelation, higher polymerization extent resulting in highly mesoporous materials (P/C = 800) or even macroporous (P/C = 1500), which further presented less defected—a more ordered—structure, as evidenced by XPS and Raman spectroscopy. Similarly, the use of acetone as solvent led to slower gelation and more structured carbon materials, this synthesis parameter had a lower impact on carbon properties than the amount of catalyst. The synthesized materials also presented some differences in their surface chemistry. XPS deconvolution of Pt 4f band evidenced a negative influence of the presence of acidic carboxylic groups on the surface of the carbon materials, on the effectiveness of the impregnation and reduction procedure. XRD evidenced higher Pt crystal size (5.1–8.4 nm) in catalysts prepared using the low polymerized and less ordered carbon xerogels, whereas Pt crystal sizes around 3.5 nm were measured for the carbon materials possessing lower concentration of defects in their structure.

With respect to the catalytic activity of these carbon xerogel-based Pt-catalysts in the electrochemical oxygen reduction reaction (ORR), defects in the structure of the support favored Pt dispersion and resulted in higher values of electrochemically active surface area (ECSA), both before and after the accelerated degradation tests. On the other hand, more ordered supports resulted in higher values of specific activity, due to enhanced metal-support interaction when using carbon materials with a lower concentration of defects, which was most probably due to an increased presence of effectively reduced Pt on their surface. In terms of mass activity, however, carbon xerogels with intermediate properties resulted in higher activity and are interesting for both distribution of particles and activity reasons. With respect to catalysts stability upon the accelerated degradation tests, the catalyst based on the carbon xerogel with a high ordering degree presented the lowest loss of activity, due to enhanced stabilization of the metallic particles. Consequently, the appropriate carbon support must not be selected only in terms of initial activity, but after also considering the expected life-time of the fuel cell.

Acknowledgments

The authors want to thank the Spanish Ministry of Economy and Competitiveness (Secretaría de Estado de I+D+I, previously Spanish Ministry of Science and Innovation) and FEDER for finantial support under the project CTQ2011-28913-C02-01. M.E. Gálvez is indebted as well to the Spanish Ministry of Economy and Competitiveness (Secretaria de Estado de I+D+i) for her "Ramón y Cajal" contract.

Conflict of Interest

The authors declare no conflict of interest.

References

1. Pekala, R.W. Organic aerogels from the polycondensation of resorcinol with formaldehyde. *J. Mater. Sci.* **1989**, *24*, 3221–3227.
2. Al-Muhtaseb, S.A.; Ritter, J.A. Preparation and Properties of Resorcinol-Formaldehyde Organic and Carbon Gels. *Adv. Mater.* **2003**, *15*, 101–114.
3. Gomes, H.T.; Samant, P.V.; Serp, P.; Kalck, P.; Figueiredo, J.L.; Faria, J.L. Carbon nanotubes and xerogels as supports of well-dispersed Pt catalysts for environmental applications. *Appl. Catal. B* **2004**, *54*, 175–182.
4. Job, N.; Thery, A.; Pirard, R.; Marien, J.; Kocon, L.; Rouzaud, J.N.; Beguin, F.; Pirard, J.P. Carbon aerogels, cryogels and xerogels: Influence of the drying method on the textural properties of porous carbon materials. *Carbon* **2005**, *43*, 2481–2494.
5. Zeng, J.; Francia, C.; Dumitrescu, M.A.; Monteverde, A.H.A.; Ijeri, V.S.; Specchia, S.; Spinelli, P. Electrochemical Performance of Pt-Based Catalysts Supported on Different Ordered Mesoporous Carbons (Pt/OMCs) for Oxygen Reduction Reaction. *Ind. Eng. Chem. Res.* **2012**, *51*, 7500–7509.
6. Zeng, J.; Francia, C.; Gerbaldi, C.; Dumitrescu, M.A.; Specchia, S.; Spinelli, P. Smart synthesis of hollow core mesoporous shell carbons (HCMSC) as effective catalyst supports for methanol oxidation and oxygen reduction reactions. *J. Solid State Electrochem.* **2012**, *16*, 3087–3096.
7. Jaouen, F.; Lefevre, M.; Dodelet, J.P.; Cai, M. Heat-Treated Fe/N/C Catalysts for O_2 Electroreduction: Are Active Sites Hosted in Micropores? *J. Phys. Chem. B* **2006**, *110*, 5553–5558.
8. Jaouen, F.; Proietti, E.; Lefevre, M.; Chenitz, R.; Dodelet, J.P.; Wu, G.; Chung, H.T.; Johnston, C.M.; Zelenay, P. Recent advances in non-precious metal catalysis for oxygen-reduction reaction in polymer electrolyte fuel cells. *Energy Environ. Sci.* **2011**, *4*, 114–130.
9. Du, H.; Li, B.; Kang, F.; Fu, R.; Zeng, Y. Carbon aerogel supported Pt–Ru catalysts for using as the anode of direct methanol fuel cells. *Carbon* **2007**, *45*, 429–435.
10. Antolini, E. Carbon supports for low-temperature fuel cell catalysts. *Appl. Catal. B* **2009**, *88*, 1–24.
11. Liang, C.; Li, Z.; Dai, S. Mesoporous Carbon Materials: Synthesis and Modification. *Angew. Chem. Int. Ed.* **2008**, *47*, 3696–3717.
12. Arbizzani, C.; Beninati, S.; Manferrari, E.; Soavi, F.; Mastragostino, M. Electrodeposited PtRu on cryogel carbon–Nafion supports for DMFC anode. *J. Power Sources* **2006**, *161*, 826–830.

13. Job, N.; Marie, J.; Lambert, S.; Berthon-Fabry, S.; Achard, P. Carbon xerogels as catalyst supports for PEM fuel cell cathode. *Energy Convers. Manag.* **2008**, *49*, 2461–2470.
14. Job, N.; Lambert, S.; Chatenet, M.; Gommes, C.J.; Maillard, F.; Berthon-Fabry, S.; Regalbuto, J.R.; Pirard, J.P. Preparation of highly loaded Pt/carbon xerogel catalysts for Proton Exchange Membrane fuel cells by the Strong Electrostatic Adsorption method. *Catal. Today* **2010**, *150*, 119–127.
15. Guilminot, E.; Fischer, F.; Chatenet, M.; Rigacci, A.; Berthon-Fabry, S.; Achard, P.; Chainet, E. Use of cellulose-based carbon aerogels as catalyst support for PEM fuel cell electrodes: Electrochemical characterization. *J. Power Sources* **2007**, *166*, 104–111.
16. Liu, B.; Creager, S. Carbon xerogels as Pt catalyst supports for polymer electrolyte membrane fuel-cell applications. *J. Power Sources* **2010**, *195*, 1812–1820.
17. Tamon, H.; Ishizaka, H.; Mikami, M.; Okazaki, M. Porous structure of organic and carbon aerogels synthesized by sol-gel polycondensation of resorcinol with formaldehyde. *Carbon* **1997**, *35*, 791–796.
18. Maldonado-Hódar, F.J.; Ferro-García, M.A.; Rivera-Utrilla, J.; Moreno-Castilla, C. Synthesis and textural characteristics of organic aerogels, transition-metal-containing organic aerogels and their carbonized derivatives. *Carbon* **1999**, *37*, 1199–1205.
19. Sharma, C.S.; Kulkarni, M.M.; Sharma, A.; Madou, A. Synthesis of carbon xerogel particles and fractal-like structures. *Chem. Eng. Sci.* **2009**, *64*, 1536–1543.
20. Job, N.; Pirard, R.; Marien, J.; Pirard, J.P. Porous carbon xerogels with texture tailored by pH control during sol–gel process. *Carbon* **2004**, *42*, 619–628.
21. Mir, L.E.; Kraiem, S.; Bengagi, M.; Elaloui, E.; Ouederni, A.; Alaya, S. Synthesis and characterization of electrical conducting nanoporous carbon structures. *Physica B* **2007**, *395*, 104–110.
22. Hernández-Fernández, P.; Montiel, M.; Ocón, P.; de la Fuente, J.L.G.; García-Rodríguez, S.; Rojas, S.; Fierro, J.L.G. Functionalization of multi-walled carbon nanotubes and application as supports for electrocatalysts in proton-exchange membrane fuel cell. *Appl Catal. B* **2010**, *99*, 343–352
23. Bustin, R.M.; Ross, J.V.; Rouzaud, J.N. Mechanisms of graphite formation from kerogen: Experimental evidence. *Int. J. Coal Geol.* **1995**, *28*, 1–36.
24. Lázaro, M.J.; Gálvez, M.E.; Artal, S.; Palacios, J.M.; Moliner, R. Preparation of steam-activated carbons as catalyst supports. *J. Anal. Appl. Pyrolysis* **2007**, *78*, 301–315.
25. Alegre, C.; Gálvez, M.E.; Baquedano, E.; Pastor, E.; Moliner, R.; Lázaro, M.J. Influence of support's oxygen functionalization on the activity of Pt/carbon xerogels catalysts for methanol electro-oxidation. *Int. J. Hydrog. Energy* **2012**, *37*, 7180–7191.
26. Velázquez-Palenzuela, F.; Centellas, J.A.; Garrido, C.; Arias, R.M.; Rodríguez, E.; Brillas, P.-L. Cabot Structural properties of unsupported pt−ru nanoparticles as anodic catalyst for proton exchange membrane fuel cells. *J. Phys. Chem. C* **2010**, *11*, 4399–4407.
27. Raman, R.K.; Shukla, A.K.; Gayen, A.; Hegde, M.S.; Priolkar, K.R.; Sarode, P.R.; Emura, S. Tailoring a Pt–Ru catalyst for enhanced methanol electro-oxidation. *J. Power Sources* **2006**, *157*, 45–55.

28. De la Fuente, J.L.G.; Martínez-Huerta, M.V.; Rojas, S.; Hernández-Fernández, P.; Terreros, P.; Fierro, J.L.G.; Peña, M.A. Tailoring and structure of PtRu nanoparticles supported on functionalized carbon for DMFC applications: New evidence of the hydrous ruthenium oxide phase. *Appl. Catal. B* **2009**, *88*, 505–514.
29. Aricò, A.S.; Antonucci, V.; Antonucci, P.L. *Metal-Support Interaction in Low-Temperature Fuel Cell Electrocatalysts in Catalysis and Electrocatalysis at Nanoparticle Surfaces*; Wieckowski, A., Savinova, E.R., Vayenas, C.G., Eds.; Marcel Dekker Inc.: New York, NY, USA, 2003; pp. 613–643.
30. Kinoshita, K. Particle Size Effects for Oxygen Reduction on Highly Dispersed Platinum in Acid Electrolytes. *J. Electrochem. Soc.* **1990**, *137*, 845–848.
31. Aricò, A.S.; Stassi, A.; Modica, E.; Ornelas, R.; Gatto, I.; Passalacqua, E.; Antonucci, V. Performance and degradation of high temperature polymer electrolyte fuel cell catalysts. *J. Power Sources* **2008**, *178*, 525–536.
32. Sebastián, D.; Ruiz, A.G.; Suelves, I.; Moliner, R.; Lázaro, M.J.; Baglio, V.; Stassi, A.; Aricò, A.S. Enhanced oxygen reduction activity and durability of Pt catalysts supported on carbon nanofibers. *Appl. Catal. B* **2012**, *115–116*, 269–275.
33. Figueiredo, J.L.; Pereira, M.F.R.; Freitas, M.M.A.; Orfao, J.J.M. Modification of the surface chemistry of activated carbons. *Carbon* **1999**, *37*, 1379–1389.
34. Sebastián, D.; Suelves, I.; Moliner, R.; Lázaro, M.J. The effect of the functionalization of carbon nanofibers on their electronic conductivity. *Carbon* **2010**, *48*, 4421–4431.
35. Baglio, V.; di Blasi, A.; Aricò, A.; Antonucci, V.; Antonucci, P.L.; Nannetti, F.; Tricoli, V. Investigation of the electrochemical behaviour in DMFCs of chabazite and clinoptilolite-based composite membranes. *Electrochim. Acta* **2005**, *50*, 5181–5188.
36. Borup, R.; Meyers, J.; Pivovar, B.; Kim, Y.S.; Mukundan, R.; Garland, N.; Meyers, D.; Wilson, M.; Garzon, F.; Wood, D.; *et al.* Scientific Aspects of Polymer Electrolyte Fuel Cell Durability and Degradation. *Chem. Rev.* **2007**, *107*, 3904–3951.